



Article

# Aquacobalamin Accelerates Orange II Destruction by Peroxymonosulfate via the Transient Formation of Secocorrinoid: A Mechanistic Study

Iliia A. Dereven'kov , Ekaterina S. Sakharova, Vladimir S. Osokin and Sergei V. Makarov \*

Department of Food Chemistry, Ivanovo State University of Chemistry and Technology, Sheremetevskiy Str. 7, 153000 Ivanovo, Russia

\* Correspondence: makarov@isuct.ru

**Abstract:** Besides its use in medicine, vitamin B<sub>12</sub> (cobalamin) and its derivatives have found in numerous applications as catalysts. However, studies related to the activation of oxidants via cobalamin are scant. In this work, we showed how the addition of aquacobalamin (H<sub>2</sub>OCbl) accelerates the destruction of azo-dye Orange II by peroxymonosulfate (HSO<sub>5</sub><sup>−</sup>) in aqueous solutions. In neutral and weakly alkaline media, the process is initiated by the modification of the corrin macrocycle with HSO<sub>5</sub><sup>−</sup>, which requires the preliminary deprotonation of the aqua-ligand in H<sub>2</sub>OCbl to give hydroxocobalamin, producing 5,6-dioxo-5,6-secocobalamin or its isomer (14,15-dioxo-14,15-secocobalamin). In acidic solutions, where the concentration of hydroxocobalamin is negligible, the formation of dioxo-seco-species is not observed, and the reaction between H<sub>2</sub>OCbl and HSO<sub>5</sub><sup>−</sup> results in slow chromophore bleaching. Using terephthalic acid, we demonstrated the formation of hydroxyl radicals in the mixture of H<sub>2</sub>OCbl with HSO<sub>5</sub><sup>−</sup>, whereas the generation of sulfate radicals was proved by comparing the effects of ethanol and nitrobenzene on Orange II destruction using the H<sub>2</sub>OCbl/HSO<sub>5</sub><sup>−</sup> system. The reaction mechanism includes the binding of HSO<sub>5</sub><sup>−</sup> to the Co(III) ion of dioxo-secocobalamin, which results in its deprotonation and the labilization of the O-O bond, leading to the formation of sulfate and hydroxyl radicals which further react with Orange II.

**Keywords:** peroxymonosulfate; vitamin B<sub>12</sub>; aquacobalamin; azo-dyes; oxidation



**Citation:** Dereven'kov, I.A.; Sakharova, E.S.; Osokin, V.S.; Makarov, S.V. Aquacobalamin Accelerates Orange II Destruction by Peroxymonosulfate via the Transient Formation of Secocorrinoid: A Mechanistic Study. *Int. J. Mol. Sci.* **2022**, *23*, 11907. <https://doi.org/10.3390/ijms231911907>

Academic Editor: Dongho Kim

Received: 3 September 2022

Accepted: 5 October 2022

Published: 7 October 2022

**Publisher's Note:** MDPI stays neutral with regard to jurisdictional claims in published maps and institutional affiliations.



**Copyright:** © 2022 by the authors. Licensee MDPI, Basel, Switzerland. This article is an open access article distributed under the terms and conditions of the Creative Commons Attribution (CC BY) license (<https://creativecommons.org/licenses/by/4.0/>).

## 1. Introduction

Peroxymonosulfate (HSO<sub>5</sub><sup>−</sup>) is a frequently used ion in advanced oxidation processes due to its ability to generate sulfate radicals (SO<sub>4</sub><sup>•−</sup>) [1,2]. SO<sub>4</sub><sup>•−</sup> exhibits extremely high oxidizing properties [3], i.e., the oxidation potential is 2.5–3.1 V (vs. a normal hydrogen electrode, NHE) [4], and is capable of reacting with numerous organic and inorganic molecules [3,5]. Cobalt compounds efficiently activate the O-O bond in HSO<sub>5</sub><sup>−</sup> [6]. It was suggested that cobalt species act as a Fenton reagent in the reaction with HSO<sub>5</sub><sup>−</sup> [6]. However, the most recent explanation of the mechanism of Co(II)-assisted HSO<sub>5</sub><sup>−</sup> activation includes the consequent binding of two SO<sub>5</sub><sup>2−</sup> molecules which results in O-O bond labilization in one of SO<sub>5</sub><sup>2−</sup> ligands, and the liberation of sulfate radicals [7]. Another study demonstrates the pronounced oxidizing properties of the Co(II)-SO<sub>5</sub><sup>2−</sup> complex as a primary intermediate in the Co(II)/peroxymonosulfate system [8]. Cobalt tetrapyrrolic complexes have been used in the activation of peroxymonosulfate as well. For example, cobalt phthalocyanine immobilized onto cellulose fiber demonstrated high efficiency in the decolorization of azo-dyes by HSO<sub>5</sub><sup>−</sup>, which increased upon the addition of bicarbonate. The catalytic cycle included the coordination of SO<sub>5</sub><sup>2−</sup> with Co(II) and the further formation of high-valent oxo-species [9]. Another study employed molecular sieves containing cobalt tetracarboxyl phthalocyanine and manganese ions for diclofenac destruction via HSO<sub>5</sub><sup>−</sup>. The process involved the generation of singlet oxygen as a major reactive oxidant as well as sulfate and hydroxyl radicals [10].

Cobalamins (Cbls; Figure 1A) are the most ubiquitous cobalt complexes in nature. The catalytic behavior of Cbls has been characterized in numerous systems [11–13]. However, the application of corrinoids in the activation of oxidants found limited attention. For example, heptamethyl cobyrinate catalyzes the oxidation of alkanes to their corresponding alcohols and ketones by *m*-chloroperbenzoic acid via the transient formation of the acylperoxido complex [14]. A complex with hydrogen peroxide has been reported for the Co(III) form of Cbl (Cbl(III)) [15], whereas the reaction of the Co(II) form of Cbl (Cbl(II)) with hydrogen peroxide leads to corrin ring modification [16,17]. Cyanocobalamin (CNCbl) was successfully used as an electrocatalyst in water oxidation [18]. The computational work suggests a relatively complex mechanism in the process, in which Cbl acts as a redox non-innocent complex [19]. CNCbl was used in the synthesis of a cobalt-containing composite, which was employed in  $\text{HSO}_5^-$  activation. However, CNCbl was subjected to pyrolysis, which resulted in the destruction of its structure [20]. In this work, we report that the addition of  $\text{H}_2\text{OCbl}$  accelerates the oxidation of azo-dye Orange II (Figure 2B) by  $\text{HSO}_5^-$  in aqueous solutions, and we provide the mechanistic details of this process. Orange II has been used earlier as a model compound in other systems, including cobalt derivatives and  $\text{HSO}_5^-$  as well [21–24].

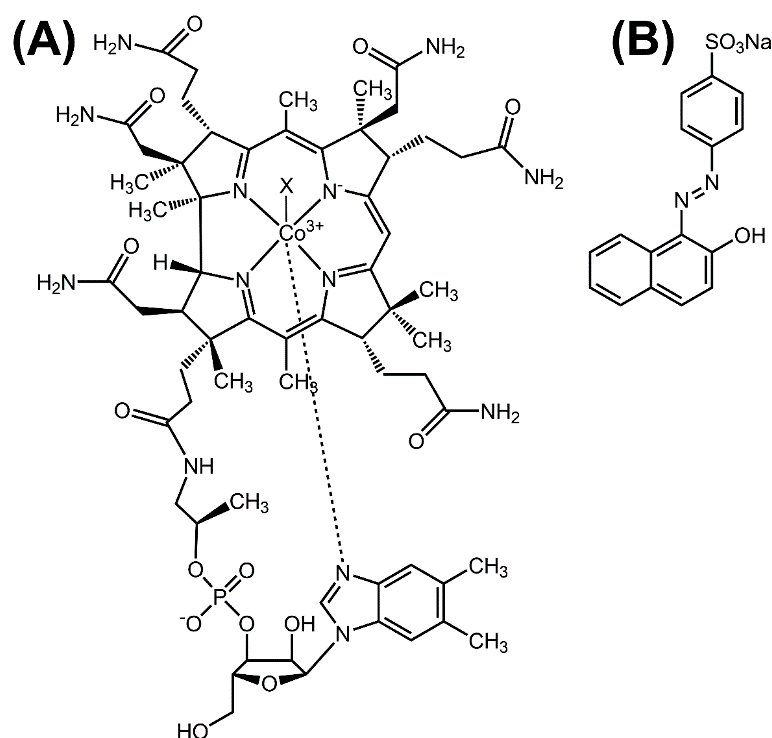


**Figure 1.** Structures of cobalamin (A; X =  $\text{H}_2\text{O}$ ;  $\text{CN}^-$  and others) and Orange II (B).

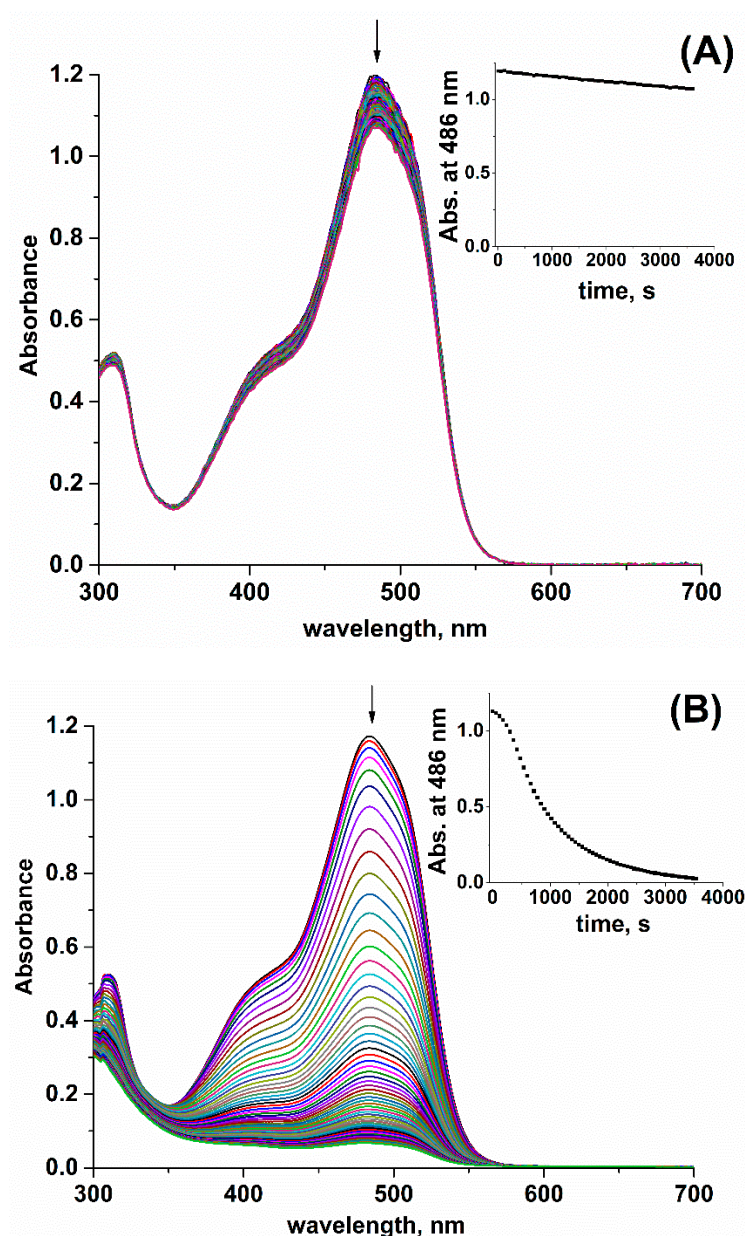


**Figure 2.** (A) UV-vis spectra of the reaction between Orange II ( $5.7 \cdot 10^{-5}$  M) and  $\text{HSO}_5^-$  ( $5.0 \cdot 10^{-4}$  M) at pH 7.4, 25.0 °C. (B) UV-vis spectra of the reaction between Orange II ( $5.7 \cdot 10^{-5}$  M) and  $\text{HSO}_5^-$  ( $5.0 \cdot 10^{-4}$  M) in the presence of  $\text{H}_2\text{OCbl}$  ( $1.0 \cdot 10^{-6}$  M) at pH 7.4, 25.0 °C. The time interval between the spectra is 60 s. The total reaction time is 60 min. Inset: time-course curves of the reactions.

## 2. Results and Discussion

Orange II bleaching by  $\text{HSO}_5^-$  proceeds slowly in a neutral medium in the absence of  $\text{H}_2\text{OCbl}$  (Figure 2A). However, the addition of  $\text{H}_2\text{OCbl}$  accelerates Orange II destruction by  $\text{HSO}_5^-$  accompanied by a decrease in the absorbance in the range between 300 and 600 nm (Figure 2B). Note that  $\text{H}_2\text{OCbl}$  ( $1.0 \cdot 10^{-6}$  M) and  $\text{HSO}_5^-$  ( $5.0 \cdot 10^{-4}$  M) weakly absorb in the UV-vis spectrum in comparison with Orange II (Supplementary Figure S1). Kinetic curves of the reaction have a sigmoid profile that can be explained by the transformation of  $\text{H}_2\text{OCbl}$  into other complexes possessing catalytic activity.

To identify catalyst species formed in the mixture of  $\text{H}_2\text{OCbl}$  with  $\text{HSO}_5^-$  and elucidate the mechanistic details of Orange II destruction in this system, we studied the reaction between  $\text{H}_2\text{OCbl}$  and  $\text{HSO}_5^-$ . Since  $\text{H}_2\text{OCbl}$  exhibits very weak absorbance in the micromolar concentration range, which was employed in most of the experiments in this

study (Supplementary Figure S1), higher  $\text{H}_2\text{OCbl}$  concentrations were used to control this process. Figure 3 shows UV-vis spectra of the reaction between  $\text{H}_2\text{OCbl}$  and the excess of  $\text{HSO}_5^-$  at pH 7.4, i.e., the formation of species with a maximum at ca. 470 nm is observed at the beginning of the reaction, when the destruction of chromophore occurs. UV-vis spectra recorded after the incubation of  $\text{H}_2\text{OCbl}$  with different concentrations of  $\text{HSO}_5^-$  indicate that  $\text{H}_2\text{OCbl}$  cannot be completely converted into the species absorbing at ca. 470 nm, which can be explained by their low stability in the presence of  $\text{HSO}_5^-$  (Supplementary Figure S2).

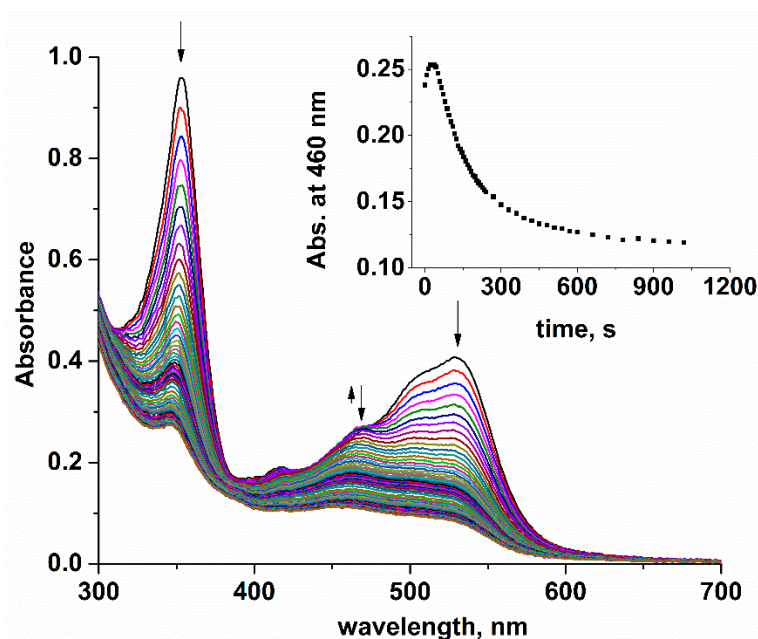


**Figure 3.** UV-vis spectra of the reaction between  $\text{H}_2\text{OCbl}$  ( $5.0 \cdot 10^{-5}$  M) and  $\text{HSO}_5^-$  ( $1.0 \cdot 10^{-3}$  M) at pH 7.4, 25.0 °C. Time intervals between the spectra are 10, 30, and 60 s for 0–4, 4.5–10 and 10–17 min of the reaction, respectively. Maxima at 353, 505, and 528 nm correspond to  $\text{H}_2\text{OCbl}$ , and maximum at ca. 470 nm—the product of  $\text{H}_2\text{OCbl}$  modification by  $\text{HSO}_5^-$  (dioxo-secocorrinoid). Inset: a time-course curve of the reaction.

The products of the reaction between  $\text{H}_2\text{OCbl}$  and the two-fold excess of  $\text{HSO}_5^-$  were separated from unreacted  $\text{H}_2\text{OCbl}$  using column chromatography. UV-vis spectrum of products is shown in Figure 4. It includes a maximum at 472 nm and lacks a  $\gamma$ -band (maximum at 300–400 nm). The same observations have been reported earlier for the reaction involving dicyanocobester and singlet oxygen photogenerated in an aerobic methanolic solution containing methylene blue, which produces a mixture of 5,6-dioxo-5,6-seco- and 14,15-dioxo-14,15-secocorrinoids (complexes with a cleaved corrin ring with a structure of 5,6-dioxo-5,6-secocobalamin are presented in Scheme 1) [25]. The formation of 5,6-dioxo-5,6-seco- or 14,15-dioxo-14,15-secocorrinoids in the course of the reaction between  $\text{H}_2\text{OCbl}$  and  $\text{HSO}_5^-$  is supported by MALDI-mass-spectroscopy as well. The mass-spectrum of the products includes a major peak at  $m/z = 1383.5$  (Supplementary Figure S3), which can be attributed to the  $[\text{Cbl}(\text{II}) - \text{H} + \text{Na} + 2\text{O}]^+$  ion corresponding to dioxo-seco-Cbl. A minor peak in the mass-spectrum at  $m/z = 1399.5$  can be assigned to hydroxylated dioxo-seco-Cbl, i.e., a product of the further reaction between dioxo-seco-Cbl and  $\text{HSO}_5^-$ .

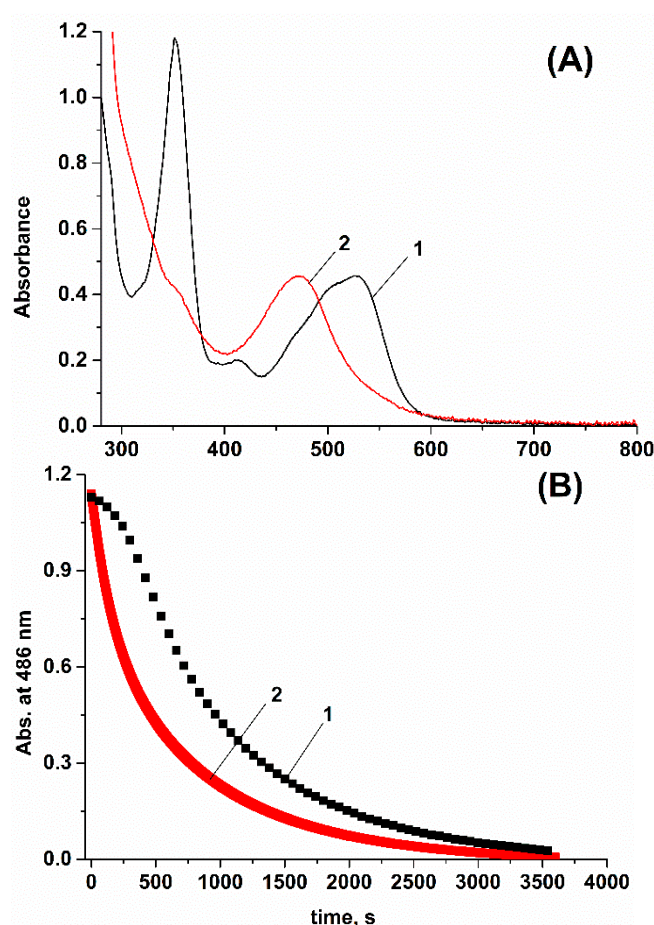
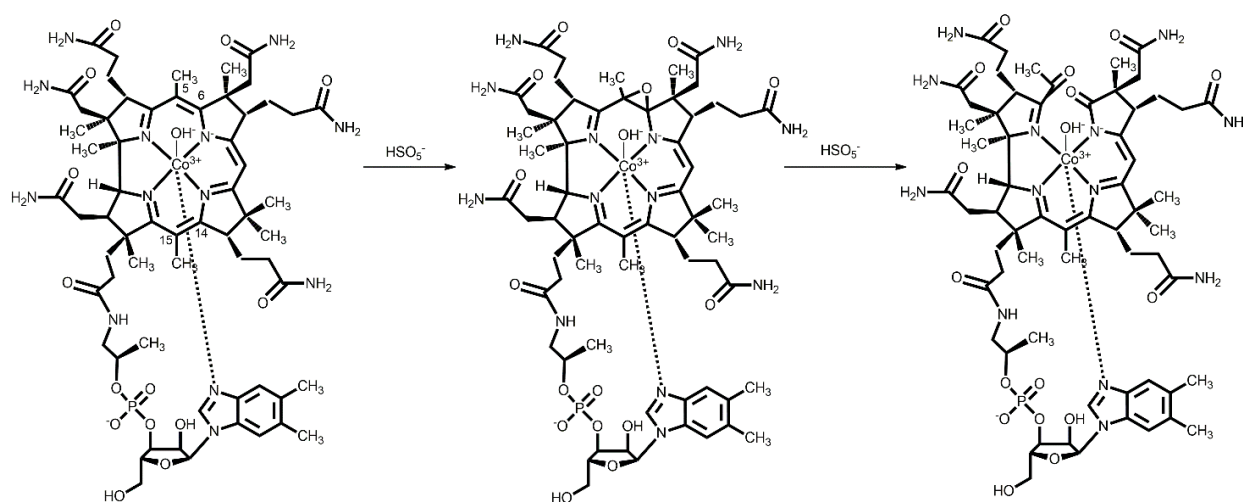


**Figure 4.** (A) UV-vis spectra of H<sub>2</sub>OCbl ( $5.0 \cdot 10^{-5}$  M; spectrum 1) and the products generated by the reaction between H<sub>2</sub>OCbl and the two-fold excess of HSO<sub>5</sub><sup>-</sup> (spectrum 2), recorded at pH 7.4, 25.0 °C. (B) Time-course curves of the Orange II ( $5.8 \cdot 10^{-5}$  M) destruction in the mixtures of HSO<sub>5</sub><sup>-</sup> ( $5.0 \cdot 10^{-4}$  M) with H<sub>2</sub>OCbl ( $1.0 \cdot 10^{-6}$  M; curve 1) and the products generated by the reaction between H<sub>2</sub>OCbl and the two-fold excess of HSO<sub>5</sub><sup>-</sup> (ca.  $1.0 \cdot 10^{-6}$  M; curve 2) at pH 7.4, 25.0 °C.



**Scheme 1.** Mechanism of hydroxocobalamin modification by HSO<sub>5</sub><sup>-</sup>. Similar parallel reactions proceed with a double bond between the C14 and C15 atoms of the corrin ring as well.

The maximum in the UV-vis spectrum of H<sub>2</sub>OCbl modification by HSO<sub>5</sub><sup>-</sup> at 472 nm can be erroneously ascribed to yellow corrinoids, i.e., corrinoid derivatives hydroxylated

at the C5- or C15-position of the corrin ring and lacking double bonds between the C4-C5 and C5-C6 or C14-C15 and C15-C16 atoms. However, UV-vis spectra of yellow corrinoids exhibit a  $\gamma$ -band, which is slightly less intense in comparison with the band of unmodified corrinoids [26,27].

The kinetic curves of Orange II bleaching in mixtures containing  $\text{HSO}_5^-$  and  $\text{H}_2\text{OCbl}$  or its dioxo-seco derivatives are shown in Figure 4. In the case of the dioxo-seco derivatives of  $\text{H}_2\text{OCbl}$ , the Orange II destruction proceeds faster and kinetic curves do not include the induction period that supports the involvement of dioxo-seco derivatives in Orange II destruction by  $\text{HSO}_5^-$ .

The intensity of the absorption maximum in the UV-vis spectrum is characteristic of dioxo-secocorrinoids (472 nm), emerging upon  $\text{H}_2\text{OCbl}$  mixing with  $\text{HSO}_5^-$ , depending on the pH. At pH 4.5, this peak is negligible (Supplementary Figure S4), and slow chromophore bleaching occurs. The peak at 472 nm becomes more pronounced in a neutral medium (Figure 3) and reaches the highest intensity at pH 9.2 (Supplementary Figure S5). This observation can be explained by the transformation of  $\text{H}_2\text{OCbl}$  to hydroxocobalamin ( $\text{pK}_a(\text{H}_2\text{OCbl}) = 7.8$  at  $25.0^\circ\text{C}$  [28]), which is capable of reacting with  $\text{HSO}_5^-$  to give dioxo-secocorrinoids. In an acidic medium, Cbl exists in an aqua-form, which reacts with  $\text{HSO}_5^-$  via chromophore degradation. In comparison with water molecules, hydroxide possesses more pronounced nucleophilic properties and likely increases the electron density of the macrocycle, which facilitates its modification with  $\text{HSO}_5^-$ . The effect of the upper-axial ligands of Cbls on the structure and yield of corrin-modified species has been reported in earlier work [29].

The reaction between  $\text{H}_2\text{OCbl}$  and  $\text{HSO}_5^-$  is almost unaffected by the addition of ethanol, which acts as a scavenger of hydroxyl [30,31] and sulfate [32] radicals generated upon O-O bond homolysis in  $\text{HSO}_5^-$  (Supplementary Figure S6). The activation of  $\text{HSO}_5^-$  can result in the formation of singlet oxygen [33,34] reacting with  $\text{H}_2\text{OCbl}$  to give dioxo-secocorrinoids [26]. However, the addition of tryptophan, an efficient quencher of singlet oxygen [35], does not affect the reaction between  $\text{H}_2\text{OCbl}$  and  $\text{HSO}_5^-$  (Supplementary Figure S7), i.e., participation of singlet dioxygen in the process is unlikely. Therefore, hydroxocobalamin is modified by  $\text{HSO}_5^-$  but not by its decomposition products. Obviously, hydroxocobalamin subsequently reacts with two  $\text{HSO}_5^-$  molecules via the epoxidation of C5-C6 or C14-C15 bonds and their further cleavage (Scheme 1).

Next, we studied the kinetics of Orange II destruction in the presence of  $\text{HSO}_5^-$  and  $\text{H}_2\text{OCbl}$ . The dependence of the maximum rate of the reaction on the initial  $\text{H}_2\text{OCbl}$  concentration is shown in Supplementary Figure S8. It is non-linear and reaches a plateau at  $[\text{H}_2\text{OCbl}] > 2.0 \cdot 10^{-5}$  M. This observation can be explained by the decomposition of catalyst species and by  $\text{HSO}_5^-$  disproportionation that becomes more pronounced in the presence of high  $\text{H}_2\text{OCbl}$  concentrations. The maximum rate of Orange II destruction by  $\text{HSO}_5^-$  in the presence of  $\text{H}_2\text{OCbl}$  linearly depends on the  $\text{HSO}_5^-$  concentration (Figure 5A). This implies that the catalyst reacts with one  $\text{HSO}_5^-$  molecule upon the generation of an oxidant reacting with the dye. The dependence of the maximum rate of Orange II oxidation by  $\text{HSO}_5^-$  in the presence of  $\text{H}_2\text{OCbl}$  on pH is shown in Figure 5B. It exhibits a bell-shaped profile with a maximum at ca. pH 8 that results from the influence of two acid-base equilibria on the reaction kinetics. One of these equilibria includes the formation of hydroxocobalamin ( $\text{pK}_a(\text{H}_2\text{OCbl}) = 7.8$  at  $25.0^\circ\text{C}$  [28]) that facilitates the formation of dioxo-secocobalamins upon an increase in pH. The second one is a deprotonation of  $\text{HSO}_5^-$  ( $\text{pK}_a = 9.3$  at  $25.0^\circ\text{C}$  [34]) that decreases its stability [1].

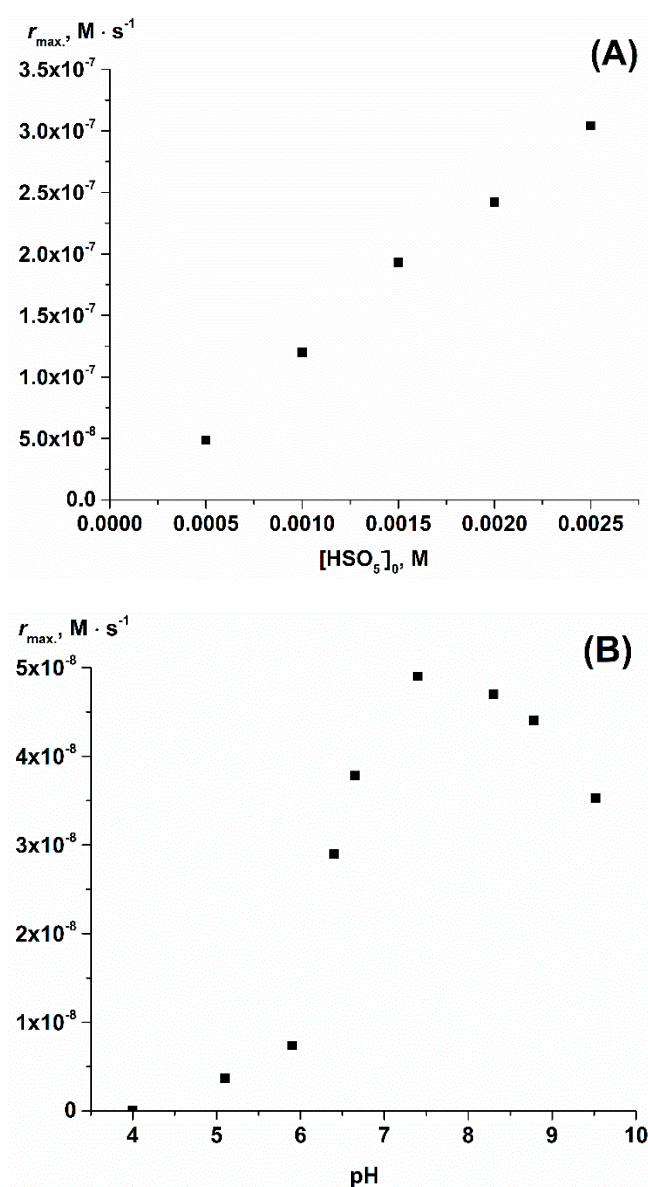


**Figure 5.** (A) The plot of the maximum rate of the reaction between Orange II ( $5.7 \cdot 10^{-5}$  M) and  $HSO_5^-$  in the presence of  $H_2OCbl$  ( $1.0 \cdot 10^{-6}$  M) versus the initial concentration of  $HSO_5^-$  at pH 7.4, 25.0 °C. (B) The plot of the maximum rate of the reaction between Orange II ( $5.7 \cdot 10^{-5}$  M) and  $HSO_5^-$  ( $5.0 \cdot 10^{-4}$  M) in the presence of  $H_2OCbl$  ( $1.0 \cdot 10^{-6}$  M) versus pH at 25.0 °C.

Using low concentrations of  $HSO_5^-$  to prevent the rapid formation of dioxo-secocorrinoids, we determined the initial rates of Orange II bleaching mediated by  $H_2OCbl$ , but not by the products of its decomposition. The dependence of the initial rate on  $HSO_5^-$  is linear (Supplementary Figure S9) with the slope  $(2.2 \pm 0.2) \cdot 10^{-5} s^{-1}$  (pH 7.4, 25.0 °C). For the dependence presented in Figure 5A, which predominantly reflects the reaction mediated by dioxo-secocorrinoids, the slope is  $(1.3 \pm 0.1) \cdot 10^{-4} s^{-1}$  (pH 7.4, 25.0 °C). Thus, the reaction mediated by dioxo-secocobalamin is ca. 10-fold more efficient than by  $H_2OCbl$ .

We attempted to identify those species formed from  $HSO_5^-$  that are responsible for the reaction with Orange II in the course of activation via dioxo-secocobalamins. The formation of hydroxyl radicals can be monitored using terephthalic acid, which produces, during this process, highly fluorescent 2-hydroxyterephthalic acid (Supplementary Figure S10) [36,37]. Indeed, 2-hydroxyterephthalic acid is generated in the mixture of terephthalic acid with  $HSO_5^-$  in the absence or in the presence of  $H_2OCbl$ . However, the addition of  $H_2OCbl$  noticeably accelerates its formation (Figure 6). Alternatively,

the formation of 2-hydroxyterephthalic acid can be suggested via a route involving the generation of singlet oxygen from the  $\text{HSO}_5^-$  peroxidation of terephthalic acid and the decomposition of the peroxides. To elucidate the type of species hydroxylating terephthalic acid, we examined the effect of ethanol on 2-hydroxyterephthalic acid formation in the abovementioned systems. Ethanol does not react with singlet oxygen in contrast to the hydroxyl radical [30,31]. We found that the addition of ethanol significantly decreases the fluorescence intensity of the 2-hydroxyterephthalic acid generated from terephthalic acid and  $\text{HSO}_5^-$  or  $\text{HSO}_5^-/\text{H}_2\text{OCbl}$  systems (Supplementary Figure S11), which supports the formation of the hydroxyl radical.

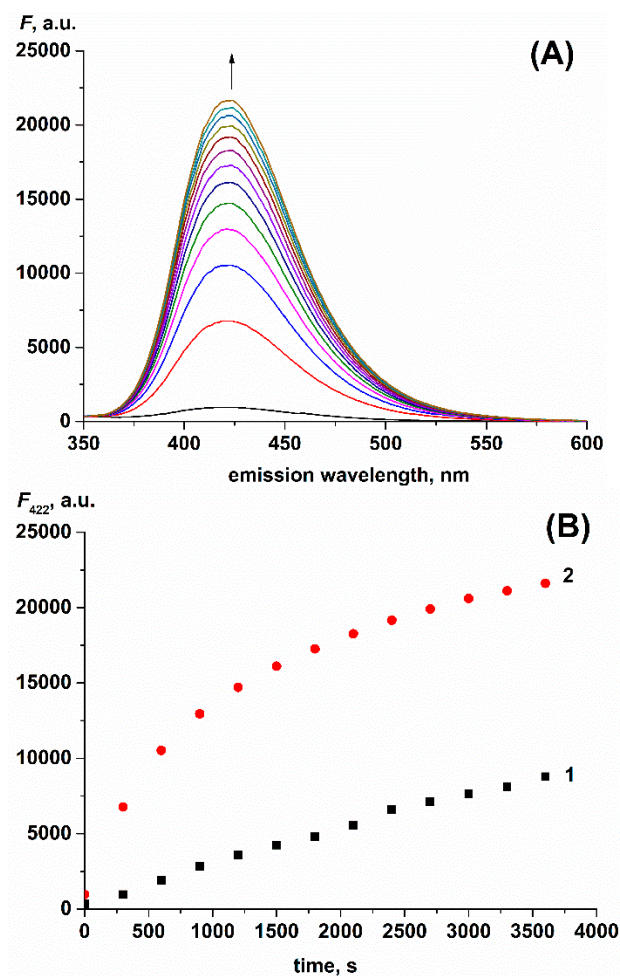


**Figure 6.** Fluorescence emission spectra of the mixture of terephthalic acid ( $1.0 \cdot 10^{-3}$  M) with  $\text{H}_2\text{OCbl}$  ( $1.0 \cdot 10^{-6}$  M) and  $\text{HSO}_5^-$  ( $5.0 \cdot 10^{-4}$  M) were recorded every 5 min after mixing (A), and plots of fluorescence intensity at 422 nm versus time for mixtures of terephthalic acid ( $1.0 \cdot 10^{-3}$  M) with  $\text{HSO}_5^-$  ( $5.0 \cdot 10^{-4}$  M; Line 1) and with  $\text{HSO}_5^-$  ( $5.0 \cdot 10^{-4}$  M) and  $\text{H}_2\text{OCbl}$  ( $1.0 \cdot 10^{-6}$  M; Line 2; B) at pH 7.4, 25.0 °C.

We compared the effect of equal concentrations of ethanol and nitrobenzene on Orange II bleaching in the presence of  $\text{H}_2\text{OCbl}$  and  $\text{HSO}_5^-$  since hydroxyl and sulfate radicals possess comparable reactivity toward ethanol, whereas the sulfate radical is less reactive toward nitrobenzene [38] than to the hydroxyl radical [39,40]. Figure 7 indicates that inhibition of the reaction is more pronounced in the case of ethanol than in the presence of nitrobenzene. This result suggests the generation of the sulfate radical upon  $\text{HSO}_5^-$  activation via the dioxo-secocobalamins.

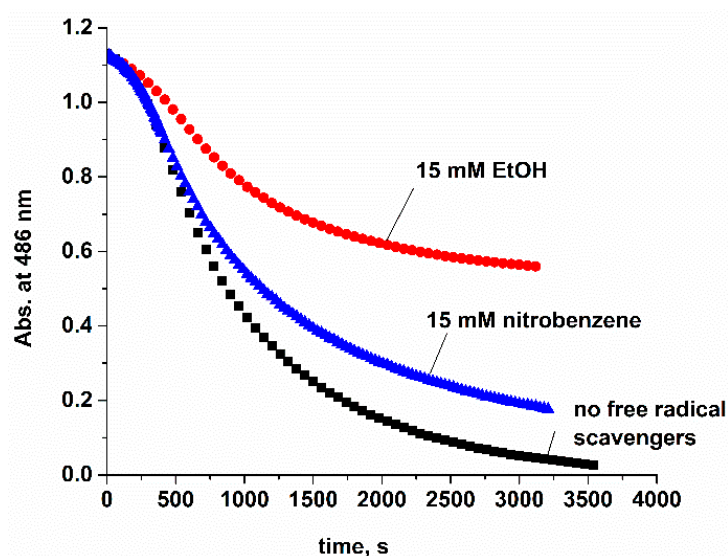
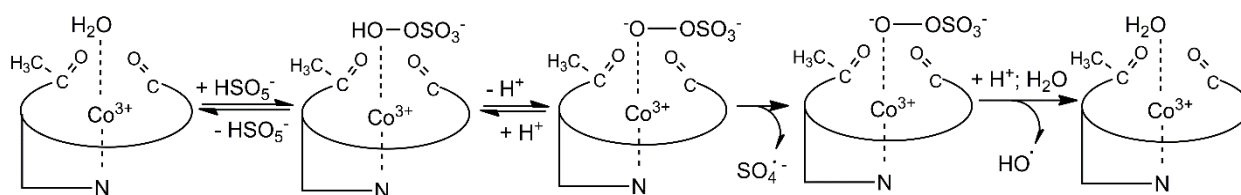


**Figure 7.** Time-course curves for Orange II ( $5.5 \cdot 10^{-5}$  M) destruction via the mixture of  $\text{H}_2\text{OCbl}$  ( $1.0 \cdot 10^{-6}$  M) with  $\text{HSO}_5^-$  ( $5.0 \cdot 10^{-4}$  M) at pH 7.4,  $25.0^\circ\text{C}$  in the absence or in the presence of ethanol ( $1.5 \cdot 10^{-2}$  M) or nitrobenzene ( $1.5 \cdot 10^{-2}$  M).

The phosphate ions used to maintain pH in the course of the experiments in this work may affect reactions involving peroxymonosulfate [41]. However, phosphate buffer concentration weakly affects the kinetics of Orange II bleaching by the  $\text{H}_2\text{OCbl}/\text{HSO}_5^-$  system (Supplementary Figure S12). A more significant effect was observed in the case of the bicarbonate ion, i.e., the addition of  $\text{HCO}_3^-$  substantially decreases the rate of Orange II destruction via the mixture of  $\text{HSO}_5^-$  with  $\text{H}_2\text{OCbl}$  in a neutral medium (Supplementary Figure S13), which can be explained by the rapid scavenging of  $\text{HO}^\bullet$  [40,42] and  $\text{SO}_4^{\bullet-}$  [43] by  $\text{HCO}_3^-$  to give a carbonate radical less reactive toward Orange II.

Thus,  $\text{HO}^\bullet$  and  $\text{SO}_4^{\bullet-}$  are formed upon  $\text{HSO}_5^-$  activation via dioxo-secocobalamins. Probably, the binding of  $\text{HSO}_5^-$  via the Co(III) ion of dioxo-secocobalamins facilitates its deprotonation and labilization of the O-O bond (Scheme 2). It is well known that the Co(III) ion in Cbls exhibits a relatively soft metal center [26,44], whereas corrin ring cleavage to give the dioxo-seco species makes the Co(III) ion harder [45]. Therefore, the coordination of  $\text{HSO}_5^-$ , a hard base, is more plausible on the Co(III) ion in dioxo-seco-Cbl than in unmodified Cbl.



**Scheme 2.** Mechanism of  $\text{HSO}_5^-$  activation by dioxo-secocobalamins.

In contrast to  $\text{H}_2\text{OCbl}$ ,  $\text{CNCbl}$  weakly affects the rate of Orange II destruction in the presence of  $\text{HSO}_5^-$  (Supplementary Figure S14). The UV-vis spectra indicate that the modification of  $\text{CNCbl}$  occurs via  $\text{HSO}_5^-$  (Supplementary Figure S15). However, no new maxima at 470–500 nm, typical to dioxo-secocorrinoids, were observed. Moreover, cyanide remains tightly bound with the Co(III) ion upon corrin modification [46] and prevents the reaction of  $\text{HSO}_5^-$  with Co(III) to generate species that react with Orange II.

Thus, this work showed that the destruction of azo dye Orange II is accelerated after the addition of aquacobalamin. Aquacobalamin retains its catalytic properties even after partial destruction. Moreover, an increase in the catalytic properties of  $\text{H}_2\text{OCbl}$  is observed upon its partial destruction, i.e., dioxo-secocorrinoids can be more efficient oxidation

catalysts in the activation of the peroxo species. Thus, the elaboration of the catalytic effect of modified corrinoids is the prospective topic for further studies.

### 3. Materials and Methods

Hydroxocobalamin hydrochloride (Sigma, St. Louis, MO, USA; HOCbl;  $\geq 96\%$ ), Oxone (Sigma;  $2\text{KHSO}_5 \cdot \text{K}_2\text{SO}_4 \cdot \text{KHSO}_4$ ), terephthalic acid (TA; Sigma-Aldrich, St. Louis, MO, USA;  $98\%$ ), 2-hydroxyterephthalic acid (J&K), Orange II sodium salt (Sigma-Aldrich;  $\geq 85\%$ ) were used without additional purification. The content of  $\text{KHSO}_5$  in OXONE was determined by the reported procedure [7]. Concentrations of Cbl stock solutions were determined using UV-visible spectroscopy via conversion of Cbl to its dicyano-form (extinction coefficient is  $30,400 \text{ M}^{-1} \cdot \text{cm}^{-1}$  at  $368 \text{ nm}$  [47]).

Buffer solutions (phosphate or its mixture with acetate or tetraborate;  $0.1 \text{ M}$ ) were used to maintain pH during the measurements. The pH values of the solutions were determined using Multitest IPL-103 pH-meter (SEMICO) equipped with an ESK-10601/7 electrode (Izmeritelnaya tekhnika) filled with  $3.0 \text{ M}$  KCl solution. The electrode was preliminarily calibrated using standard buffer solutions (pH 1.65–12.45).

Ultraviolet-visible (UV-vis) spectra were recorded on a cryothermostated ( $\pm 0.1 \text{ }^\circ\text{C}$ ) Shimadzu UV-1800 and Cary 50 UV-Vis spectrophotometers in quartz cells.

Fluorescence emission spectra were recorded on a Shimadzu RF-6000 spectrofluorophotometer. The excitation wavelength was  $315 \text{ nm}$ , and the excitation and emission bandwidths were  $1.5$  and  $20.0 \text{ nm}$ , respectively.

Separation of products of the reaction between  $\text{H}_2\text{OCbl}$  and the two-fold excess of  $\text{HSO}_5^-$  at pH 7.4 from unreacted  $\text{H}_2\text{OCbl}$  was performed using column chromatography on silica gel (Sigma-Aldrich; average pore size  $60 \text{ \AA}$  ( $52\text{--}73 \text{ \AA}$ ),  $70\text{--}230$  mesh,  $63\text{--}200 \text{ }\mu\text{m}$ ) using  $5\%$  aqueous acetic acid as eluent.

MALDI-MS measurements were performed on a Shimadzu AXIMA Confidence mass-spectrometer with 2,5-dihydroxybenzoic acid as the matrix.

### 4. Conclusions

This work demonstrated that the bleaching of azo-dye Orange II by  $\text{HSO}_5^-$  is accelerated upon the addition of aquacobalamin. The reaction between hydroxocobalamin and  $\text{HSO}_5^-$  results in corrin ring cleavage and the formation of 5,6-dioxo-5,6-secocobalamin, which participates in the activation of  $\text{HSO}_5^-$ . The mixing together of aquacobalamin with  $\text{HSO}_5^-$  and terephthalic acid generates 2-hydroxyterephthalic acid more efficiently than in the absence of  $\text{H}_2\text{OCbl}$ , indicating the formation of hydroxyl radicals. In the presence of ethanol, which acts as an efficient scavenger of hydroxyl and sulfate radicals, the bleaching of the Orange II by the  $\text{H}_2\text{OCbl}/\text{HSO}_5^-$  mixture proceeds less efficiently, whereas, with the effect of nitrobenzene, which is less reactive toward  $\text{SO}_4^{\bullet-}$  than it is toward  $\text{HO}^\bullet$ , the inhibition of the reaction was less pronounced. These results confirm the important role of  $\text{SO}_4^{\bullet-}$  in the destruction of Orange II. The strong inhibition of Orange II bleaching was observed upon adding bicarbonate to the  $\text{H}_2\text{OCbl}/\text{HSO}_5^-$  system; this can be explained by the reaction of  $\text{HCO}_3^-$  with  $\text{SO}_4^{\bullet-}$  and  $\text{HO}^\bullet$  to give a less reactive carbonate radical. The suggested mechanism of  $\text{HSO}_5^-$  activation by dioxo-secocobalamin includes the formation of a complex between the Co(III) ion and  $\text{HSO}_5^-$  which leads to peroxymonosulfate deprotonation and the labilization of the O-O bond, also resulting in the formation of the hydroxyl and sulfate radicals. In contrast to  $\text{H}_2\text{OCbl}$ , cyanocobalamin weakly affects the rate of Orange II bleaching by  $\text{HSO}_5^-$ , which can be explained by the absence of dioxo-secocorrinoid formation upon the reaction of cyanocobalamin with  $\text{HSO}_5^-$ , as well as by the presence of cyanide bound to cobalt in cobalamin-derived species, preventing the reaction between the cobalt ions and  $\text{HSO}_5^-$ .

**Supplementary Materials:** The following supporting information can be downloaded at: <https://www.mdpi.com/article/10.3390/ijms231911907/s1>. Figure S1. UV-vis spectra of Orange II ( $5.7 \cdot 10^{-5} \text{ M}$ ),  $\text{H}_2\text{OCbl}$  ( $1.0 \cdot 10^{-6} \text{ M}$ ) and  $\text{HSO}_5^-$  ( $5.0 \cdot 10^{-4} \text{ M}$ ) at pH 7.4,  $25.0 \text{ }^\circ\text{C}$ ; Figure S2. UV-vis spectra of the mixtures of  $\text{H}_2\text{OCbl}$  ( $5.0 \cdot 10^{-5} \text{ M}$ ) with different quantities of  $\text{HSO}_5^-$  recorded after

5 hours of incubation at pH 7.4, 25.0 °C; Figure S3. MALDI-mass-spectrum of the products of the reaction between H<sub>2</sub>OCl and two-fold excess of HSO<sup>5-</sup>; Figure S4. UV-vis spectra of the reaction between H<sub>2</sub>OCl (5.0·10<sup>-5</sup> M) and HSO<sup>5-</sup> (1.0·10<sup>-3</sup> M) at pH 4.5, 25.0 °C; Figure S5. UV-vis spectra of the reaction between H<sub>2</sub>OCl (5.0·10<sup>-5</sup> M) and HSO<sup>5-</sup> (1.0·10<sup>-3</sup> M) at pH 9.2, 25.0 °C. Figure S6. UV-vis spectra for the reaction between H<sub>2</sub>OCl (5.0·10<sup>-5</sup> M) with HSO<sup>5-</sup> (1.0·10<sup>-3</sup> M) at pH 7.4, 25.0 °C in the presence of ethanol (5.0·10<sup>-2</sup> M); Figure S7. UV-vis spectra for the reaction between H<sub>2</sub>OCl (5.0·10<sup>-5</sup> M) with HSO<sup>5-</sup> (1.0·10<sup>-3</sup> M) at pH 7.4, 25.0 °C in the presence of tryptophan (5.0·10<sup>-3</sup> M). Figure S8. Plot of the maximum rate of the reaction between Orange II (5.7·10<sup>-5</sup> M) and HSO<sup>5-</sup> (5.0·10<sup>-4</sup> M) in the presence of H<sub>2</sub>OCl versus initial concentration of H<sub>2</sub>OCl at pH 7.4, 25.0 °C; Figure S9. Plot of the initial rate of the reaction between Orange II (5.7·10<sup>-5</sup> M) and HSO<sup>5-</sup> in the presence of H<sub>2</sub>OCl (1.0·10<sup>-6</sup> M) versus initial concentration of HSO<sup>5-</sup> at pH 7.4, 25.0 °C; Figure S10. Fluorescence emission spectrum of 2-hydroxyterephthalic acid (1.0·10<sup>-6</sup> M) at pH 7.4, 25.0 °C; Figure S11. Plots of fluorescence intensity at 422 nm versus time for mixtures of terephthalic acid (1.0·10<sup>-3</sup> M) with HSO<sup>5-</sup> (5.0·10<sup>-4</sup> M; A) and with HSO<sup>5-</sup> (5.0·10<sup>-4</sup> M) and H<sub>2</sub>OCl (1.0·10<sup>-6</sup> M; B) in the absence and in the presence of ethanol (50 mM) at pH 7.4, 25.0 °C; Figure S12. Time-course curves for the destruction of Orange II (5.5·10<sup>-5</sup> M) by the mixture of H<sub>2</sub>OCl (1.0·10<sup>-6</sup> M) with HSO<sup>5-</sup> (5.0·10<sup>-4</sup> M) at pH 7.4, 25.0 °C in the presence of different phosphate buffer concentrations; Figure S13. UV-vis spectra for the destruction of Orange II (5.7·10<sup>-5</sup> M) by the mixture of H<sub>2</sub>OCl (1.0·10<sup>-6</sup> M) with HSO<sup>5-</sup> (5.0·10<sup>-4</sup> M) at pH 7.4, 25.0 °C in the presence of HCO<sub>3</sub><sup>-</sup> (5.0·10<sup>-2</sup> M); Figure S14. UV-vis spectra of the reaction between Orange II (5.5·10<sup>-5</sup> M) and HSO<sup>5-</sup> (5.0·10<sup>-4</sup> M) in the presence of CNCI (1.0·10<sup>-6</sup> M) at pH 7.4, 25.0 °C; Figure S15. UV-vis spectra for the reaction between CNCI (5.0·10<sup>-5</sup> M) with HSO<sup>5-</sup> (5.0·10<sup>-4</sup> M) at pH 7.0, 25.0 °C.

**Author Contributions:** I.A.D. was responsible for the investigation, funding acquisition, and writing—original draft preparation; E.S.S. and V.S.O. were responsible for investigation; S.V.M. was responsible for supervision and writing—review & editing. All authors have read and agreed to the published version of the manuscript.

**Funding:** This work was supported by the Russian Science Foundation (project no. 21-73-10057; <https://rscf.ru/project/21-73-10057/>) to IAD.

**Institutional Review Board Statement:** Not applicable.

**Informed Consent Statement:** Not applicable.

**Data Availability Statement:** Not applicable.

**Acknowledgments:** MALDI-mass-spectrometry experiments were carried out using the resources of the Center for Shared Use of Scientific Equipment of the ISUCT (with the support of the Ministry of Science and Higher Education of Russia, grant No. 075-15-2021-671).

**Conflicts of Interest:** The authors declare no conflict of interest.

## References

1. Ghanbari, F.; Moradi, M. Application of peroxymonosulfate and its activation methods for degradation of environmental organic pollutants: Review. *Chem. Eng. J.* **2017**, *310*, 41–62. [[CrossRef](#)]
2. Wang, J.; Wang, S. Activation of persulfate (PS) and peroxymonosulfate (PMS) and application for the degradation of emerging contaminants. *Chem. Eng. J.* **2018**, *334*, 1502–1517. [[CrossRef](#)]
3. Zhang, B.-T.; Zhang, Y.; Teng, Y.; Fan, M. Sulfate Radical and Its Application in Decontamination Technologies. *Crit. Rev. Environ. Sci. Technol.* **2015**, *45*, 1756–1800. [[CrossRef](#)]
4. Neta, P.; Huie, R.E.; Ross, A.B. Rate Constants for Reactions of Inorganic Radicals in Aqueous Solution. *J. Phys. Chem. Ref. Data* **1988**, *17*, 1027–1284. [[CrossRef](#)]
5. Anipsitakis, G.P.; Dionysiou, D. Degradation of Organic Contaminants in Water with Sulfate Radicals Generated by the Conjunction of Peroxymonosulfate with Cobalt, *Environ. Sci. Technol.* **2003**, *37*, 4790–4797. [[CrossRef](#)]
6. Hu, P.; Long, M. Cobalt-catalyzed sulfate radical-based advanced oxidation: A review on heterogeneous catalysts and applications. *Appl. Catal. B Environ.* **2016**, *181*, 103–117. [[CrossRef](#)]
7. Shamir, D.; Meyerstein, D.; Katsaran, D.; Pochtarenko, L.; Yardeni, G.; Burg, A.; Albo, Y.; Kornweitz, H.; Zilbermann, I. Mechanisms of Reaction Between Co(II) Complexes and Peroxymonosulfate. *Eur. J. Inorg. Chem.* **2022**, e202100646. [[CrossRef](#)]
8. Li, H.; Zhao, Z.; Qian, J.; Pan, B. Are Free Radicals the Primary Reactive Species in Co(II)-Mediated Activation of Peroxymonosulfate? New Evidence for the Role of the Co(II)–Peroxymonosulfate Complex. *Environ. Sci. Technol.* **2021**, *55*, 6397–6406. [[CrossRef](#)]

9. Huang, Z.; Yao, Y.; Lu, J.; Chen, C.; Lu, W.; Huang, S.; Chen, W. The consortium of heterogeneous cobalt phthalocyanine catalyst and bicarbonate ion as a novel platform for contaminants elimination based on peroxymonosulfate activation. *J. Hazard. Mater.* **2016**, *301*, 214–221. [[CrossRef](#)]
10. Wu, M.; Fu, K.; Deng, H.; Shi, J. Cobalt tetracarboxyl phthalocyanine-manganese octahedral molecular sieve (OMS-2) as a heterogeneous catalyst of peroxymonosulfate for degradation of diclofenac. *Chemosphere* **2019**, *219*, 756–765. [[CrossRef](#)]
11. Giedyk, M.; Golszewska, K.; Gryko, D. Vitamin B<sub>12</sub> catalysed reactions. *Chem. Soc. Rev.* **2015**, *44*, 3391–3404. [[CrossRef](#)] [[PubMed](#)]
12. Koide, T.; Ono, T.; Shimakoshi, H.; Hisaeda, Y. Functions of bioinspired pyrrole cobalt complexes—recently developed catalytic systems of vitamin B<sub>12</sub> related complexes and porphycene complexes. *Coord. Chem. Rev.* **2022**, *472*, 214690. [[CrossRef](#)]
13. Dereven'kov, I.A.; Salnikov, D.S.; Silaghi-Dumitrescu, R.; Makarov, S.V.; Koifman, O.I. Redox chemistry of cobalamin and its derivatives. *Coord. Chem. Rev.* **2016**, *309*, 68–83. [[CrossRef](#)]
14. Cheng, J.; Shiota, Y.; Yamasaki, M.; Izukawa, K.; Tachi, Y.; Yoshizawa, K.; Shimakoshi, H. Mechanistic Study for the Reaction of B<sub>12</sub> Complexes with m-Chloroperbenzoic Acid in Catalytic Alkane Oxidations. *Inorg. Chem.* **2022**, *61*, 9710–9724. [[CrossRef](#)]
15. Lehene, M.; Plesa, D.; Ionescu-Zinca, S.; Iancu, S.D.; Leopold, N.; Makarov, S.V.; Brânzanic, A.M.V.; Silaghi-Dumitrescu, R. Adduct of Aquacobalamin with Hydrogen Peroxide. *Inorg. Chem.* **2021**, *60*, 12681–12684. [[CrossRef](#)]
16. Salnikov, D.S.; Makarov, S.V.; Koifman, O.I. The radical versus ionic mechanisms of reduced cobalamin inactivation by tert-butyl hydroperoxide and hydrogen peroxide in aqueous solution. *New J. Chem.* **2021**, *45*, 535–543. [[CrossRef](#)]
17. Dereven'kov, I.A.; Makarov, S.V.; Makarova, A.S. Mechanism of aquacobalamin decomposition in aqueous aerobic solutions containing glucose oxidase and glucose. *React. Kinet. Mech. Catal.* **2021**, *133*, 73–84. [[CrossRef](#)]
18. Shahadat, H.M.; Younus, H.A.; Ahmad, N.; Shiguo, Z.; Zhuyikov, S.; Verpoort, F. Macrocyclic cyanocobalamin (vitamin B<sub>12</sub>) as a homogeneous electrocatalyst for water oxidation under neutral conditions. *Chem. Commun.* **2020**, *56*, 1968–1971. [[CrossRef](#)]
19. Li, Y.-Y.; Liao, R.-Z. Mechanism of water oxidation catalyzed by vitamin B<sub>12</sub>: Redox non-innocent nature of corrin ligand and crucial role of phosphate. *Chin. Chem. Lett.* **2022**, *33*, 358–361. [[CrossRef](#)]
20. Hou, J.; Lin, J.; Fu, H.; Wan, Y.; Qu, X.; Xu, Z.; Zheng, S. Vitamin B<sub>12</sub> derived CoCN<sub>x</sub> composite confined in SBA-15 as highly effective catalyst to activate peroxymonosulfate for naproxen degradation. *Chem. Eng. J.* **2020**, *389*, 124344. [[CrossRef](#)]
21. Zhiyong, Y.; Bensimon, M.; Laub, D.; Kiwi-Minsker, L.; Jardim, W.; Mielczarski, E.; Mielczarski, J.; Kiwi, J. Accelerated photodegradation (minute range) of the commercial azo-dye Orange II mediated by Co<sub>3</sub>O<sub>4</sub>/Raschig rings in the presence of oxone. *J. Mol. Catal. A: Chem.* **2007**, *272*, 11–19. [[CrossRef](#)]
22. Raja, P.; Bensimon, M.; Klehm, U.; Albers, P.; Laub, D.; Kiwi-Minsker, L.; Renken, A.; Kiwi, J. Highly dispersed PTFE/Co<sub>3</sub>O<sub>4</sub> flexible films as photocatalyst showing fast kinetic performance for the discoloration of azo-dyes under solar irradiation. *J. Photochem. Photobiol. A Chem.* **2007**, *187*, 332–338. [[CrossRef](#)]
23. Shi, P.; Su, R.; Wan, F.; Zhu, M.; Li, D.; Xu, S. Co<sub>3</sub>O<sub>4</sub> nanocrystals on graphene oxide as a synergistic catalyst for degradation of Orange II in water by advanced oxidation technology based on sulfate radicals. *Appl. Catal. B: Environ.* **2012**, *123–124*, 265–272. [[CrossRef](#)]
24. Shi, P.; Su, R.; Zhu, S.; Zhu, M.; Li, D.; Xu, S. Supported cobalt oxide on graphene oxide: Highly efficient catalysts for the removal of Orange II from water. *J. Hazard. Mater.* **2012**, *229–230*, 331–339. [[CrossRef](#)]
25. Kräutler, B. The Photooxygenation of Heptamethyl Co $\alpha$ , Co $\beta$ -Dicyanocobyrinate. *Helv. Chim. Acta.* **1982**, *65*, 1941–1948. [[CrossRef](#)]
26. Chemaly, S.M.; Brown, K.L.; Fernandes, M.A.; Munro, O.Q.; Grimmer, C.; Marques, H.M. Probing the Nature of the Co<sup>III</sup> Ion in Corrins: The Structural and Electronic Properties of Dicyano- and Aquacyanocobyrinic Acid Heptamethyl Ester and a Stable Yellow Dicyano- and Aquacyanocobyrinic Acid Heptamethyl Ester. *Inorg. Chem.* **2011**, *50*, 8700–8718. [[CrossRef](#)]
27. Pugina, R.A.; Denisova, E.A.; Ivlev, P.A.; Salnikov, D.S.; Makarov, S.V. Synthesis of vitamin B<sub>12</sub> derivatives with sodium hydroxymethanesulfinate. *J. Porphyr. Phthalocyanines* **2018**, *22*, 1092–1098. [[CrossRef](#)]
28. Xia, L.; Cregan, A.G.; Berben, L.A.; Brasch, N.E. Studies on the Formation of Glutathionylcobalamin: Any Free Intracellular Aquacobalamin Is Likely to Be Rapidly and Irreversibly Converted to Glutathionylcobalamin. *Inorg. Chem.* **2004**, *43*, 6848–6857. [[CrossRef](#)]
29. Wagner, F. Reactions of the cyano and alkyl cobalamins. *Proc. R. Soc. A* **1965**, *288*, 344–347. [[CrossRef](#)]
30. Kwon, B.G.; Ryu, S.; Yoon, J. Determination of hydroxyl radical rate constants in a continuous flow system using competition kinetics. *J. Ind. Eng. Chem.* **2009**, *15*, 809–812. [[CrossRef](#)]
31. Thomas, J.K. Rates of Reaction of the Hydroxyl Radical. *Trans. Faraday Soc.* **1965**, *61*, 702–707. [[CrossRef](#)]
32. Clifton, C.L.; Huie, R.E. Rate constants for hydrogen abstraction reactions of the sulfate radical, SO<sub>4</sub><sup>-</sup>. Alcohols. *Int. J. Chem. Kin.* **1989**, *21*, 677–687. [[CrossRef](#)]
33. Xiao, G.; Xu, T.; Faheem, M.; Xi, Y.; Zhou, T.; Moryani, H.T.; Bao, J.; Du, J. Evolution of Singlet Oxygen by Activating Peroxydisulfate and Peroxymonosulfate: A Review. *Int. J. Environ. Res. Public Health* **2021**, *18*, 3344. [[CrossRef](#)] [[PubMed](#)]
34. Evans, D.F.; Upton, M.W. Studies on singlet oxygen in aqueous solution. Part 3. The decomposition of peroxy-acids. *J. Chem. Soc. Dalton Trans.* **1985**, 1151–1153. [[CrossRef](#)]
35. Matheson, I.B.C.; Lee, J. Chemical reaction rates of amino acids with singlet oxygen. *Photochem. Photobiol.* **1979**, *29*, 879–881. [[CrossRef](#)]
36. Charbouillot, T.; Brigante, M.; Mailhot, G.; Maddigapu, P.R.; Minero, C.; Vione, D. Performance and selectivity of the terephthalic acid probe for radical •OH as a function of temperature, pH and composition of atmospherically relevant aqueous media. *J. Photochem. Photobiol. A Chem.* **2011**, *222*, 70–76. [[CrossRef](#)]

37. Dereven'kov, I.A.; Makarov, S.V.; Brânzanic, A.M.V.; Silaghi-Dumitrescu, R.; Molodtsov, P.A.; Pokrovskaya, E.A. Formation of hydroxyl radical in aqueous solutions containing selenite and glutathione. *Polyhedron* **2021**, *198*, 115072. [[CrossRef](#)]
38. Neta, P.; Madhavan, V.; Zemel, H.; Fessenden, R.W. Rate constants and mechanism of the reaction of sulfate radical anion with aromatic compounds. *J. Am. Chem. Soc.* **1977**, *99*, 163–164. [[CrossRef](#)]
39. Matthews, R.W.; Sangster, D.F. Measurement by Benzoate Radiolytic Decarboxylation of Relative Rate Constants for Hydroxyl Radical Reactions. *J. Phys. Chem.* **1965**, *69*, 1938–1946. [[CrossRef](#)]
40. Hoigné, J.; Bader, H. The role of hydroxyl radical reactions in ozonation processes in aqueous solutions. *Water Res.* **1976**, *10*, 377–386. [[CrossRef](#)]
41. Duan, P.; Liu, X.; Liu, B.; Akram, M.; Li, Y.; Pan, J.; Yue, Q.; Gao, B.; Xu, X. Effect of phosphate on peroxymonosulfate activation: Accelerating generation of sulfate radical and underlying mechanism. *Appl. Catal. B Environ.* **2021**, *298*, 120532. [[CrossRef](#)]
42. Weeks, J.T.; Rabani, J.J. The Pulse Radiolysis of Deaerated Aqueous Carbonate Solutions. I. Transient Optical Spectrum and Mechanism. II. pK for OH Radicals. *J. Phys. Chem.* **1966**, *70*, 2100–2106. [[CrossRef](#)]
43. Dogliotti, L.; Hayon, E. Flash photolysis of per[oxydi]sulfate ions in aqueous solutions. The sulfate and ozonide radical anions. *J. Phys. Chem.* **1967**, *71*, 2511–2516. [[CrossRef](#)]
44. Perry, C.B.; Fernandes, M.A.; Brown, K.L.; Zou, X.; Valente, E.J.; Marques, H.M. Probing the Nature of the Co<sup>III</sup> Ion in Cobalamins – Spectroscopic and Structural Investigations of the Reactions of Aquacobalamin (Vitamin B<sub>12a</sub>) with Ambident Nucleophiles. *Eur. J. Inorg. Chem.* **2003**, 2095–2107. [[CrossRef](#)]
45. Nowakowska, M.; Chemaly, S.M.; Rousseau, A.L.; Govender, P.P.; Varadwaj, P.R.; Varadwaj, A.; Yamashita, K.; Marques, H.M. Probing the nature of the Co(III) ion in corrins: The reactions of aquacyano-5-seco-cobyric acid heptamethyl ester with anionic ligands. *Inorg. Chim. Acta* **2019**, *484*, 402–413. [[CrossRef](#)]
46. Salnikov, D.S.; Dereven'kov, I.A.; Artyushina, E.N.; Makarov, S.V. Interaction of cyanocobalamin with sulfur-containing reducing agents in aqueous solutions. *Russ. J. Phys. Chem. A* **2013**, *87*, 44–48. [[CrossRef](#)]
47. Barker, H.A.; Smyth, R.D.; Weissbach, H.; Toohey, J.I.; Ladd, J.N.; Volcani, B.E. Isolation and Properties of Crystalline Cobamide Coenzymes Containing Benzimidazole or 5,6-Dimethylbenzimidazole. *J. Biol. Chem.* **1960**, *235*, 480–488. [[CrossRef](#)]